X-ray ptychography with highly-curved wavefront

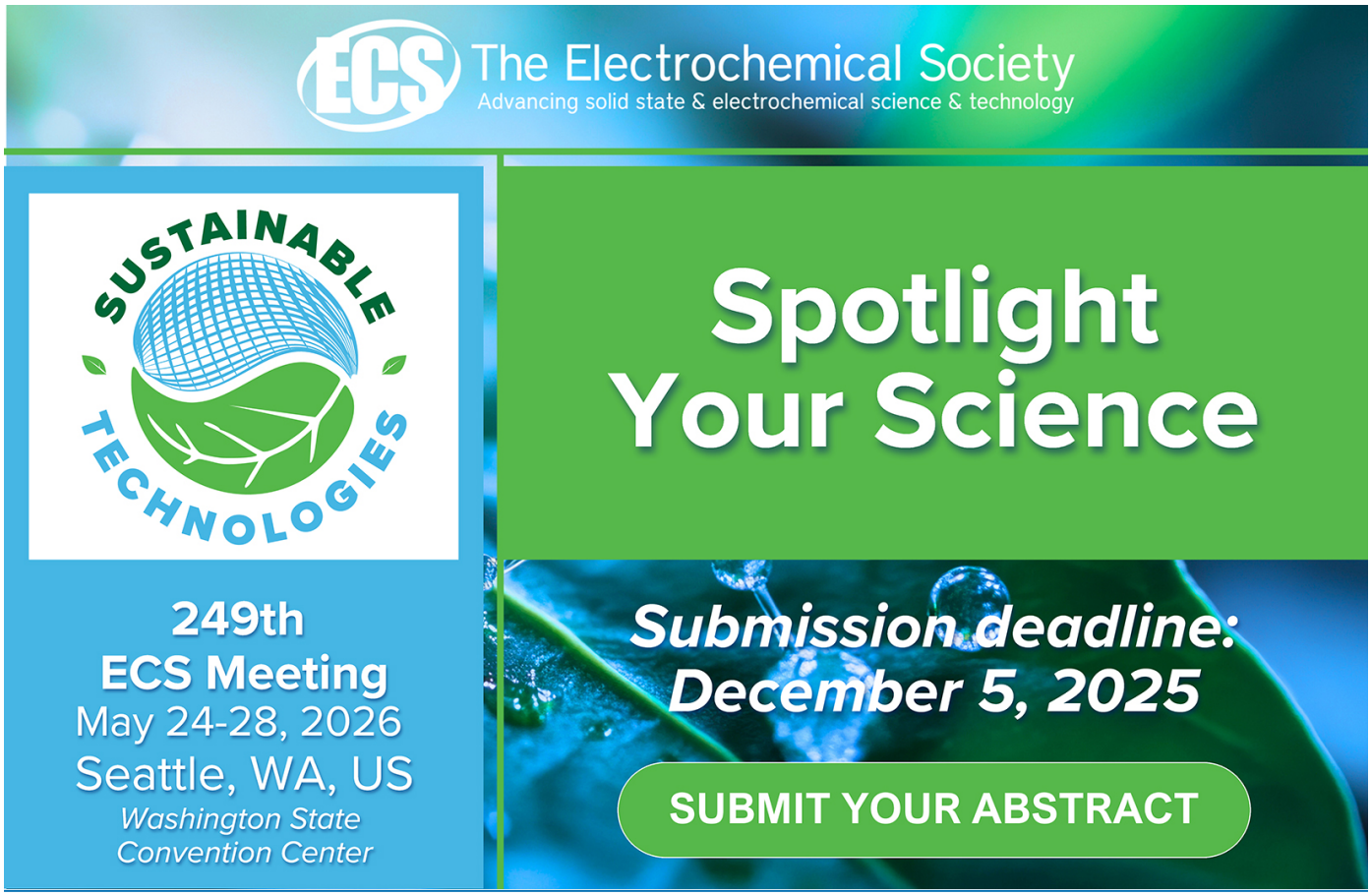

X-ray ptychography with highly-curved wavefront

S. Wang[1], D. Shapiro[2], K. Kaznatcheev[1],
[1]NSLSII, Brookhaven National Laboratory, Upton NY 11973, USA
[2]ALS, Lawerence Berkeley National Laboratory, Berkeley CA 94720, USA

E-mail: shellywang@bnl.gov

Abstract. The recent development of scanning coherent x-ay diffraction microscopy (also known as ptychography) eliminates several constraints exerted by coherent imaging. In particular, an illuminating wave (the probe) can have an arbitrary shape, as a diffraction data redundancy due to multiple measurements at overlapping neighboring probe positions permits its independent reconstruction along with the scattering potential (the object wave). A priori knowledge, such as a finite sample support, is reduced to a recording of sequential probe positions and a plausible guess to be used as a starting estimate for iterative phase retrieval. Using a focusing probe, such as one produced by a zone plate, we investigate the effectiveness of the reconstruction algorithm and find that it is significantly less successful at reconstructing wavefronts with large curvature (extended phase variation) than the wavefronts with almost flat phase structure. Our simulations show that when the actual probe has large phase variation, the amount of overlap required for a successful reconstruction of both object and probe depends upon the phase difference between the actual probe and the probe used as a starting estimate for the reconstruction. We quantitatively define the circumstances for successful reconstruction of an object placed away from focus. We use an experimental dataset measured with a moderate amount of overlap to show that a successful reconstruction of the test sample can be done using a curved probe as an initial guess.

1. Introduction.

For a successful demonstration of real-space reconstruction of a non-periodic object based on a far field diffraction pattern [1], x-ray coherent diffractive imaging (CDI) emerges as an alternative to x-ray microscopy. CDI was successfully applied to 2D [2] and 3D [3,4] fabricated nanostructures and a specimen as complex as a yeast cell [5,6,7,8]. A five orders of magnitude increase in average brightness of novel x-ray free-electron lasers further fuels the coherent scattering technique development [9,10], raising the hope that the x-ray coherent scattering will be capable of imaging complex specimens at a spatial resolution below 10nm, or beyond the quality limit given by x-ray optics [11].

As only scattering intensity is measured, the scattering wave phase has to be reconstructed via a computational procedure that at each iterative step equalizes the square modulus of the scattering wave Fourier transform to a measured diffraction intensity while phase is left to be complied with other experimental constraints [12]. As a result, many CDI experimental setups use pinhole and object reconstruction assuming plane-wave illumination. This is not ideal for soft x-rays, since pinholes scatter very strongly when used alone and, if the pinhole is not very close to the sample, the scattering pattern is large and difficult to properly record. Earlier attempts to use focusing light demonstrate an improved iterative algorithm convergence, but they still rely on a priori knowledge of the probe-wave derived from experimental geometry [13,14]. The non-uniform optic illumination and optics fabrication errors or aberrations limit the object reconstruction accuracy, as only the probe- and object-

wave product is measured. In scanning x-ray diffraction microscopy, the measurements are performed at overlapped adjacent object areas, so collected data have a redundancy. A critical advance provided by Thibault et al. was the probe retrieval step as a means of verifying the probe structure in parallel with the object reconstruction [15,16]. As a result, both self-consistent solutions of the probe- and object-waves are derived.

2. Simulations.

Numerical simulations were performed using diffraction data generated from the USAF 1951 resolution test pattern and probes with a Gaussian intensity profile and a quadratic phase term. For the area outside the three-line patch the object-wave amplitude is set to unity, at the line it is set to zero, and the phase jump is set to π. The probes, shown to the left in Figure 1, have different phase terms: flat (probe 0 with no phase variation), curved with a maximum phase variation of 100 π (probe 1), and far out-of-focus probe with a maximum phase of 200 π (probe 2). Notation "probe x-y" means that the data are generated with probe x but probe y is used as an initial guess. These probes were sampled on a grid with 128x128 pixels, so the maximum phase jump per pixel was kept well below π in all cases. A circular scan pattern of a total of 61 positions was chosen to avoid artificial square-grid aliasing, and the dose delivered to the object was varied by adjusting the spacing between grid rings. Typically, the ptychographic datasets are characterized by the probe overlap as set by the ratio of the distance between neighboring probe positions to the width of the probe [17]. However, when the probe has a complicated intensity distribution, as it does for the out-of-focus sample position of the zone plate probe, the overlap is poorly defined. Here, we define the overlap as the dose per pixel averaged over the illumination area, assuming the normalized Gaussian intensity distribution.

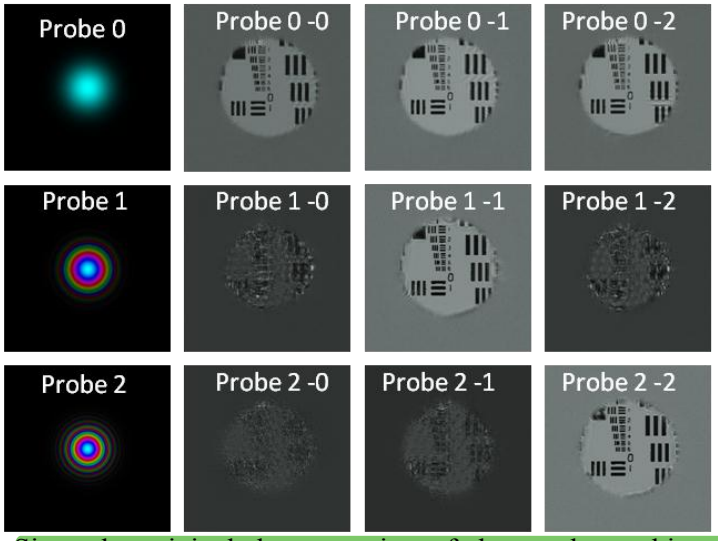

Figure 1. Reconstruction images at average dose of 0.7. Results were all obtained after 500 ePIE iteration steps. The renderings of the complex-valued reconstructions use brightness to represent the magnitude (it also applies to Figure 3 (d) and (e)). The background outside of the illumination area is darker for the unsuccessful images because of the presence of bright pixels.

Since the original demonstration of the ptychographic approach [18], several versions of phase retrieval procedures have been developed [19, 20]. We chose to follow the extended ptychographic reconstruction engine (ePIE) algorithm and use the same notation as in [21]. An update parameter β, used to seed the probe at each step, was set to 0.75 and has not been changed during the reconstruction. The object update function α was equal to 0.001. The initial guess probe is set to have the same intensity as the probe used to generate the scattering data but an incorrect phase term in a form of quadratic exponent. The reconstruction error, as a normalized difference between the square of the simulated diffraction intensity and modulus of the scattering wave Fourier transform (omitting constant phase offset) is computed after every tenth iteration and is used to determine an algorithm convergence (Figure 2).

Figure 1 shows the results of object reconstruction after 500 ePIE iterations for the dataset with 0.7 overlap. Images at the cross illustrate the result of object reconstruction where the scattering pattern is generated with one probe function but at a different initial guess. Good reconstruction is observed

across the diagonal line, where the departure of initial guess and the resulting probe is small. Data generated by the flat probe are also insensitive to initial probe-wave guess. In contrast, the data sets with large phase variation require a good estimate of initial probe. Otherwise, the algorithm converges to a wrong result.

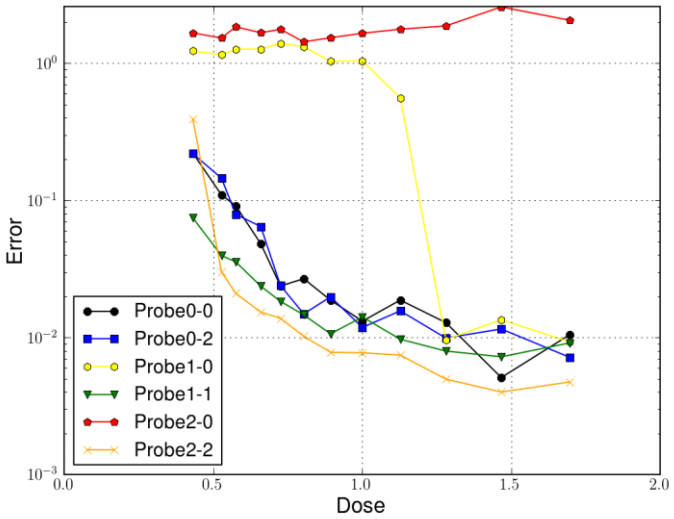

Figure 2. Error (log scale) of simulation data reconstruction after ePIE 500 iterations evolves as function of average dose for different combinations of actual probe and starting probe.

As both good initial guess and the overlap function define a degree of algorithm convergence, Figure 2 shows the result of reconstruction (represented by the error function) as a function of probe overlap (dose). For clarity, we omit some results but left one defining the trend. Our simulation shows that there is an optimum overlap (dose) range, 0.5-1.8, for a successful reconstruction to take place. At a dose below 0.5 even a good initial guess of illumination function may result in large reconstruction errors. For high dose (above 1.80, not shown), the reconstruction based on the ePIE algorithm also fails—possibly due to poor convergence. As in the case of large overlap, it might be more appropriate to use the hybrid input-output algorithm as discussed in [17].

3. Experiment.

The experimental data set was acquired using the Scanning Transmission X-ray Microscope at the Canadian Light Source ID10 beamline. The test sample of lithographically fabricated gold nano-structure consists of elbow-shaped 150nm wide lines deposited on a 100nm thick Si_3N_4 window. The sample was placed approximately 30µm downstream of the zone plate focus. At 710eV energy, for the zone plate of 240µm diameter with 25nm outermost zone, the width of the x-ray spot size was just over 2 µm. The sample was scanned on a 5x5 grid at 560 nm stepsize. Andor DX camera was located 35mm downstream of the sample. The scattering images were cropped to the central part (256x256 pixels, pixel size of 13µm) of a CCD image, providing a 12 nm pixel size of reconstructed image. The calculated dose is 0.85, which, as suggested by the simulation, is above the critical dose needed for good convergence. Figure 3 shows one of the scattering images (Figure 3 (b)) as well as two alternative initial guess probe-waves (Figure 3(a), for large phase variation, but constant intensity, consistent with 30µm out-of-focus zone plate beam, and Figure 3(c), with constant phase across ~2µm size pupil, as in pinhole probe). Only out-of-focus probe-waves result in a successful reconstruction. Note that the reconstructed probe-wave has a more donut-like shape consistent with zone plate pupil function, and it is different from the initial guess. The estimate of the gold thickness (80nm), based on tabulated x-ray cross-sections and the observed phase jump across the elbow line, is also consistent

with actual gold plated thickness (~100nm).

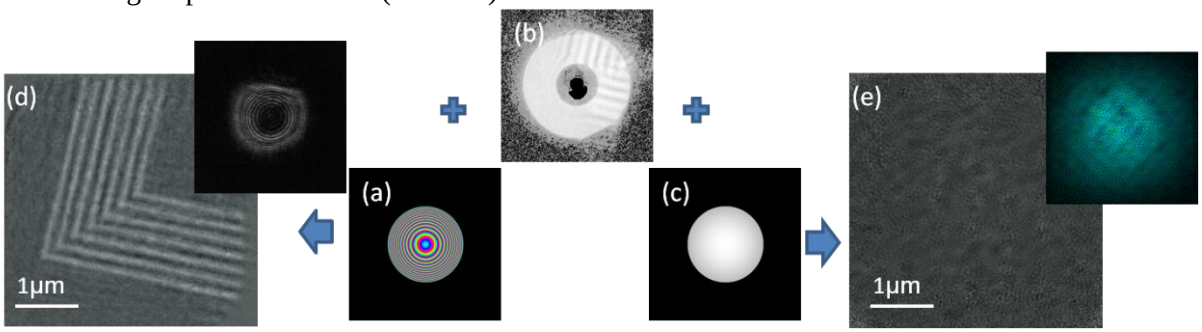

Figure 3. (a) the starting zone plate type curved probe; (b) an example scattering image (log scale); (c) the starting pin hole type probe; (d) successful reconstruction image (amplitude) and resultant probe when using probe in (a); (e) failed reconstruction image and resultant probe when using probe in (c).

4. Conclusion.

Using numerical simulation we study how ptychographical reconstruction error varies with the illumination dose for near-to-focus probe-waves. We find that the ePIE algorithm requires a more accurate initial guess of the probe when the actual probe has a large phase variation or it requires significantly higher overlap. Inaccurate guesses or insufficient overlap lead to reconstruction failure. We then demonstrate experimentally the ability to reconstruct ptychographic data with the test sample spaced away from the zone plate focus. Even a Gaussian-shaped initial probe with close to real geometry quadratic phase term was sufficient to lead to a successful test object reconstruction.

Acknowledgement.

The current work is based on BNL research development grant 11-030. The National Synchrotron Light Source II is supported by US DOE contract DE-AC02-98CH10886.

References

[1] Miao J, Charalambous P, Kirz J and Sayre D1999 *Nature* **400** 342
[2] Chapman H et al. 2006 *Nat. Phys.* **2** 839
[3] Chapman H et al. 2006 *J.Opt.Soc.Am.* A **23** 1179
[4] Barty A et al. 2008 *Phys.Rev.Lett.* **101** 055501
[5] Shapiro D et al. 2005 *PANS* **102** 15343
[6] Nelson J et al. 2010 *PNAS* **107** 7235
[7] Giewekemeyer K et al. 2010 *PNAS* **107** 529
[8] Huang X et al. 2009 *Phys. Rew. Lett.* **103** 198101
[9] Martin A V et al. 2012 *Opt. Express* **20** 13501
[10] Martin A V et al. 2012 *Opt. Express* **20** 16650
[11] Boutet S and Williams G L 2010 *New J. Phys.* **12** 035024
[12] Fienup J R 1982 *Appl. Opt.* **21** 2758
[13] Quiney H M, Peele A G, Cai Z, Paterson D and Nugent K A 2006 *Nat. Phys.* **2** 101
[14] Williams G J et al. 2010 *New J. Phys*. **12** 035020
[15] Thibault P, Dierolf M, Menzel A, Bunk O, David C, and Pfeiffer F 2008 *Science* **321** 379
[16] Rodenburg J M, Dierolf M, Kynde S, Johnson I, Marti O and Pfeiffer F 2007 *Phy. Rev.Lett.* **98** 034801.
[17] Bunk O, Dierolf M, Kynde S, Johnson I, Marti O and Pfeiffer F 2008 *Ultramicroscopy* **108** 481
[18] Rodenburg J M 2004 *App. Phys. Letters* **85** 4795
[19] Marchesini S 2007 *Rev. Sci. Instrum.* **78** 011301
[20] Yang C et al. 2011 arXiv:1105.5628
[21] Maiden A M and Rodenburg J M 2009 *Ultramicroscopy* **109** 1256